

Impact of corrosion on axial load capacity of ageing low-strength reinforced concrete columns with different confinement ratios

Hammed O. Aminulai^a, Andrew F. Robinson^b, Neil S. Ferguson^c, Mohammed M. Kashani^{d,*}

^a Department of Civil Engineering, School of Engineering, University of Southampton, United Kingdom

^b School of Engineering, TSRL Laboratory, University of Southampton, United Kingdom

^c Institute for Sounds and Vibration, School of Engineering, University of Southampton, United Kingdom

^d Department of Civil Engineering, School of Engineering, University of Southampton, United Kingdom

ARTICLE INFO

Keywords:

Axial load
Reinforced concrete column
Confinement
Corrosion
Rebar buckling

ABSTRACT

Many ageing structures in earthquake-prone regions are vulnerable to failure by seismic actions resulting from the poor detailing, environmental degradation and quality of materials used. Insufficient column confinement and corrosion of the embedded reinforcement have been identified as some of the problems existing within such structures. This paper summarises the results of an experimental investigation into ageing low-strength short-reinforced concrete (R.C.) columns with varying confinement levels and degrees of corrosion. The latter is introduced in a controlled manner using electrolysis. In total, thirty short R.C. columns (15 square and 15 circular) with three confinement ratios and steel corrosion loss (0% to ~30%) were subjected to monotonic axial load. The experimental results showed rebar buckling was more pronounced at higher corrosion rates and in sparsely confined columns. In addition, the load-carrying capacity of the R.C. columns was significantly affected by corrosion and the degree of confinement.

1. Introduction

Ageing in reinforced concrete (R.C.) structures results in the loss of their strength and capacity via a slow, progressive and irreversible process over time. In addition, the ageing process results in the degradation of their structural engineering properties by limiting the capacity and resistance to failure [1,2]. This failure is more pronounced in R.C. structures in aggressive and marine environments, potentially located in seismic regions, where the structures are subject to corrosion effects and comprise poor quality materials used in their construction.

Corrosion of reinforcement in concrete is one of the most common and dangerous environmental deteriorations affecting the structural performance of ageing structures in chloride-laden and high seismic environments [3,4]. It significantly reduces the diameter [5], strength [6] and axial load-bearing capacity of reinforcing bars in corroded R.C. structures [7–9]. Furthermore, as the corrosion products expand, it exerts tensile stresses on the interface between the reinforcement and concrete, resulting in corrosion cracks and subsequent spalling of the concrete cover [8]. This results in a reduction in the concrete core confinement leading to the degradation of strength and ductility, and the long-term performance of the R.C. structure [10,11].

Chloride-induced corrosion is devastating and significantly degrades R.C. bridges and structures, resulting in substantial economic loss worldwide [12]. For example, the United States of America reported needing about \$125 billion to repair ageing and existing bridges [13]. In comparison, the United Kingdom estimated the cost of corrosion damage to highway bridges in Wales and England (approximately 10% of the total bridges in the United Kingdom) at £1 billion per year [14].

Numerous experimental and numerical studies have been carried out on corrosion-damaged R.C. components [15–18]. Moreover, many studies have been devoted to evaluating the seismic reliability of corroded R.C. components/structures [19–23]. These studies concluded that the corrosion of the reinforcement increases the likelihood of catastrophic collapse in R.C. structures.

Ageing R.C. columns/piers generally fail through buckling the vertical reinforcement bars together with the crushing of core confined concrete and the fracture of the longitudinal bars [18], resulting from inadequate confining transverse reinforcements. The failure becomes more critical in columns/piers in corrosion-laden environments where chloride-induced corrosion is prevalent and significantly affects the stress–strain behaviour of reinforcing bars. Therefore, numerous models are proposed to investigate the axial load–displacement behaviour of R.

* Corresponding author.

E-mail address: mehdi.kashani@soton.ac.uk (M.M. Kashani).

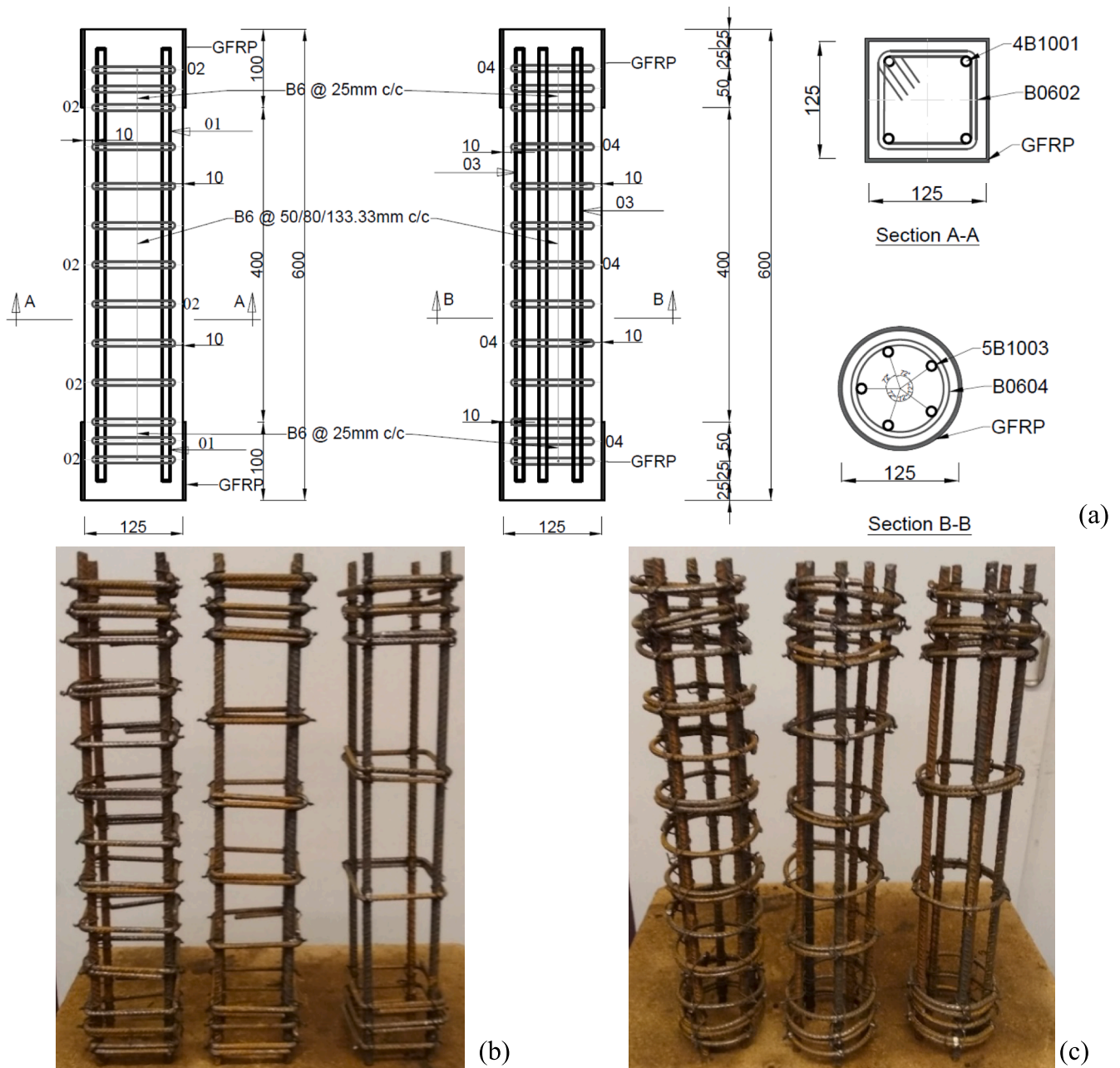


Fig. 1. Specimen details; (a) schematic drawing, (b) and (c) Reinforcement layouts (cages) of square and circular columns, respectively.

C. columns/piers in seismic regions [4,10,24–26].

In the design of R.C. bridge piers/columns to resist seismic vibrations, the plastic regions are provided with adequate transverse reinforcement to improve their ductility and strength and prevent the buckling of longitudinal bars. This confinement reinforcement provides the compressed concrete with higher flexibility and stability, which helps to prevent collapse and shear failure during vibrations [27]. Thus, the higher the level of confining stress in the concrete, the more its ductility and strength gain [28]. Several numerical and analytical models have been developed to investigate the effect of confinement of transverse reinforcement on the axial load capacity and stress–strain behaviour of R.C. columns [27–31]. However, these models are primarily on pristine R.C. columns, without considering the effect of corrosion on the structural response of columns/piers. These models have been incorporated into design guidelines and codes for designing new R.C. bridge columns/piers. However, there are still many old bridge columns with the old design without proper confinement. Therefore, the

behaviour and response of these old columns to combined effects of degradation and axial compressive load needs to be investigated.

2. Research contribution and novelty

Although the stress–strain behaviour of confined concrete in non-corroded R.C. columns has been comprehensively addressed [32], there are very few experimental studies on the effects of corrosion on the stress–strain behaviour of confined concrete columns, including the corrosion of the longitudinal bars. Several researchers have used analytically developed stress–strain models of confined concrete subjected to corrosion for numerical applications without experimental verification [33,34]. Also, most of the experimental works have been on normal and high-strength R.C. structures without any experimental testing on old R.C. structures with low-strength concrete. However, there are still many old R.C. structures having low-strength concrete in seismic regions without proper seismic detailing. Hence, it is imperative

Table 1
Experimental test matrix of the R.C. columns.

Circular columns			Square columns		
Specimen label	Confinement level	Targeted corrosion (%)	Specimen label	Confinement level	Targeted corrosion (%)
C5B0	5	0	S5B0	5	0
C5B5	5	5	S5B5	5	5
C5B10	5	10	S5B10	5	10
C5B20	5	20	S5B20	5	20
C5B30	5	30	S5B30	5	30
C8B0	8	0	S8B0	8	0
C8B5	8	5	S8A5	8	5
C8B10	8	10	S8B10	8	10
C8B20	8	20	S8B20	8	20
C8B30	8	30	S8B30	8	30
C13B0	13	0	S13B0	13	0
C13B5	13	5	S13B5	13	5
C13B10	13	10	S13B10	13	10
C13B20	13	20	S13B20	13	20
C13B30	13	30	S13B30	13	30

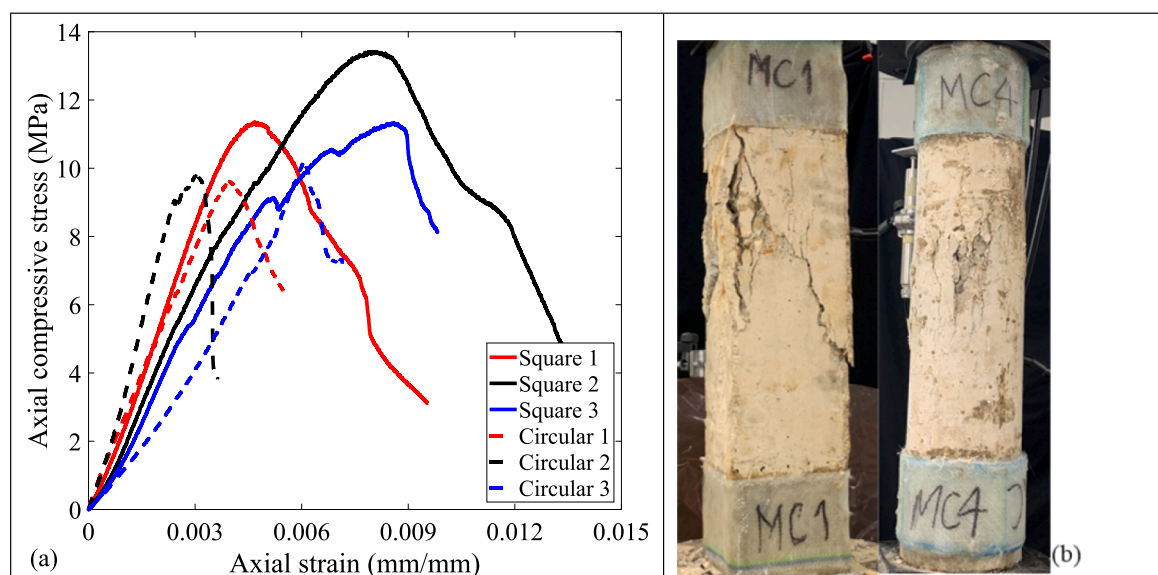


Fig. 2. Mass concrete behaviour (a) compressive stress–strain response (b) observed failure after the test.

to study the impact of corrosion on such old R.C. structures to understand their responses under load.

The corrosion of the rebars (longitudinal and transverse) in the concrete further decreases the mechanical performance of the corroded R.C. elements. As such, researchers modified some R.C. elements models to reflect the corrosion effect on the stress–strain response of degraded R.C. columns. For example, Vu et al. [4] adjusted the Mander et al. [27] equation by adding the effect of corrosion on the volumetric ratio and yield strength of the transverse confining reinforcement leading to a reduction in the adequate lateral confining pressure of the corroded column. Furthermore, Ma et al. [10] extended the Mander et al. [27] and Vu et al. [4] models to reflect the corrosion effect on transverse reinforcements in rectangular columns.

Nevertheless, in most of the studies mentioned above, the influence of corrosion of the longitudinal and transverse rebars and different confinement configurations are not considered simultaneously. The corrosion test of reinforcement generally results in the loss of mechanical strength of R.C. members, while adequate confinement improves the ductility of R.C. members. Therefore, it is imperative to investigate the performance of R.C. columns under simultaneous reinforcement corrosion of the longitudinal and transverse reinforcement and the different confinement ratios.

The present study investigated the mechanical behaviour of ageing

low-strength circular and square R.C. columns under simultaneous reinforcement corrosion, confinement configurations and monotonic axial load. 30 R.C. columns were designed and grouped into five different target degrees of reinforcement corrosion (i.e., 0%, 5%, 10%, 20% and 30%) with three confinement ratios ($L/D = 5$, $L/D = 8$ and $L/D = 13$) under monotonic axial load. The different degrees of reinforcement corrosion was obtained by an accelerated corrosion technique using the electrochemical process (Faraday's electrolysis technique). The effect of reinforcement corrosion and confinement ratios on the subsequent load-deformation responses of R.C. columns was analysed. The experimental results are further compared with existing analytical models in the literature.

3. Experimental programme

3.1. Specimen details material properties

A total of 30 R.C. columns (15 squares and 15 circulars) were designed as shown in Fig. 1 and cast into square and circular columns. The square columns have a $125 \times 125 \times 600$ mm dimension incorporating 4 No. 10 mm diameter longitudinal bars, while the circular samples (125 mm diameter \times 600 mm long) have 5 No. 10 mm longitudinal bars. All the rebars in the columns were joined together with

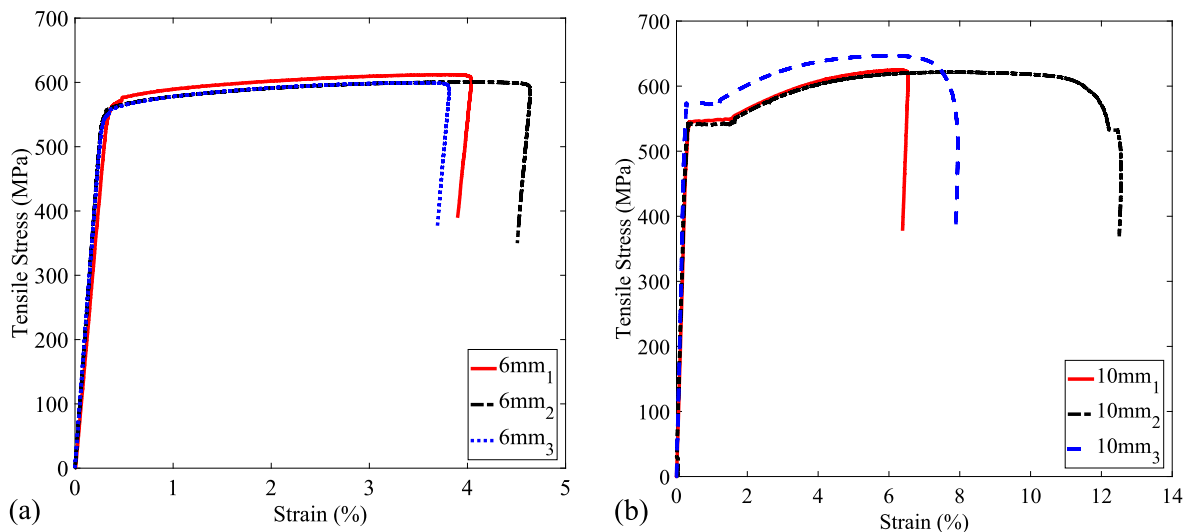


Fig. 3. Tensile stress–strain behaviour of reinforcement bars (a) transverse (b) longitudinal.

Table 2

Mechanical properties of the uncorroded transverse and longitudinal bars.

Reinforcement type	6 mm (B6)	10 mm (B10)
Yield Strength, f_y (Mpa)	531.82	551.68
Ultimate strength, f_u (Mpa)	603.05	630.11
Modulus of Elasticity, E (GPa)	185.23	196.73
Yield Strain, $\epsilon_y = f_y/E$	0.00287	0.00280
Ultimate strain, ϵ_u	0.03356	0.06349
Strain ratio, (ϵ_u/ϵ_y)	11.69	22.67
Strength ratio, (f_u/f_y)	1.134	1.142
Total elongation at maximum force, (%)	3.36	6.35
Total elongation at failure, λ_f (%)	4.16	8.49
Unit mass, m (kg/m)	0.224	0.624

Table 3

Minimum values of tensile properties of b500b reinforcement [36].

Reinforcement type	6 mm (B6)	10 mm (B10)
Yield Strength, f_y (Mpa)	485	485
Strength ratio, f_u/f_y	1.06	1.06
Total elongation at maximum force, (%)	4.0	4.0
Unit mass, m (kg/m)	0.222	0.617

steel tie wires to ensure that the transverse and longitudinal bars corrode during the corrosion process. The columns were designed with three different confinement ratios in the middle 400 mm zone, while the 100 mm ends have transverse bars spaced at 25 mm. Furthermore, the 100 mm ends are wrapped with epoxy-coated GFRP to minimise the stress concentration damage at the top and bottom ends of the columns and ensure that the failure occurs at the R.C. columns' middle zone. The test samples have three levels of confinements based on the spacing of the transverse bars, L, and the diameter of the longitudinal bar, D ($L/D = 5, 8$ and 13) and five targeted degrees of corrosion. The target degrees of corrosion range from 0% to 30% (i.e. 0%, 5%, 10%, 20% and 30%). The specimens were categorised according to the shape into square and circular (i.e. C and S), with the second numbers representing the level of confinements (5, 8 and 13) while the last numbers denote the estimated degree of corrosion (Table 1).

The concrete mix was designed as low-strength concrete representing a non-code conforming column with an expected mean compressive strength of 20 MPa and a maximum aggregate size of 10 mm. All the columns were cast with a nominal cover of 10 mm. Concrete samples with the same configuration as the square and circular columns were

taken for compressive strength tests during the casting. All of the compressive strength testing was done at the Testing and Structures Research Laboratory (TSRL), the University of Southampton, using the hydraulically powered 630kN Instron Schenk machine. The concrete columns were tested using the displacement control at a constant loading rate of 2 mm/min until failure. The samples used for the test were not the conventional cube/cylinder samples but with the same configurations as the reinforced ones. The square samples are $125 \times 125 \times 600$ mm in dimension, while the circular samples are 125 mm diameter \times 600 mm long. The strain was estimated at the middle 400 mm section same as the reinforced columns. Fig. 2(a) shows the stress–strain response of the concrete, with the square columns having an average compressive strength of 12.03 MPa while the circular columns have 9.90 MPa compressive strength. The difference in responses of different specimens is due to the differences in their failure mechanisms.

Separately, tensile tests were conducted on the uncorroded transverse and longitudinal rebars using the Instron 8032 test machine, with 100kN capacity and ± 50 mm travel, to determine the mechanical properties. Three reinforcement samples amongst the transverse and longitudinal rebars used in the columns were selected for the tensile tests according to BS EN 10080:2005 [35] and B.S. 4449:2005 + A3:2016 [36]. In addition, the rebars were subjected to different loading rates before and after the yielding as specified in BS EN ISO 6892-1:2019 [37]. At the same time, a 50 mm dynamic extensometer with ± 5 mm maximum stroke measures the strain corresponding to the extension of the rebar.

The stress–strain response of the rebars is shown in Fig. 3, while the summary of the mechanical properties and code requirements is shown in Tables 2 and 3, respectively. The average yield, ultimate strengths and strain values obtained conform to the values specified for B500B rebars [36]. Also, the variation in unit mass from the code specification (Table 3) for the 6 mm and 10 mm bars are 0.9% and 1.13% respectively, which is insignificant.

3.2. Accelerated corrosion procedure

The natural corrosion process usually takes a more extended period which could be several years or decades. As such, the electrochemical process known as the accelerated corrosion method is often adopted in the laboratory to simulate the corrosion process. Much research has been done to investigate these corrosion methods' effectiveness in reproducing R.C. structures' corrosion process. Researchers have used the constant voltage [38–41] and the constant current [42–46] methods

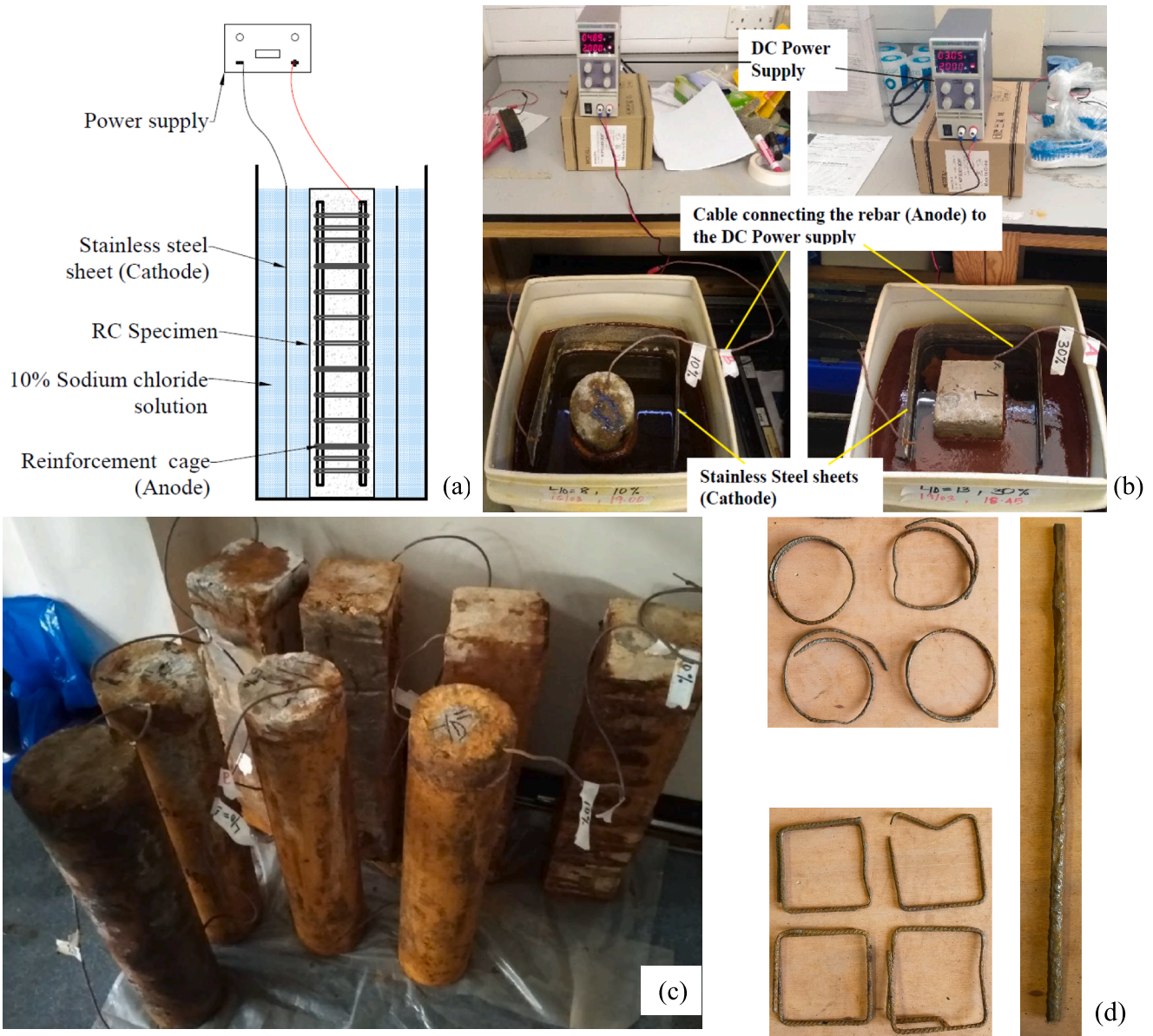


Fig. 4. Accelerated corrosion procedure; (a) Schematic setup drawing, (b) laboratory setup, (c) corroded columns, and (d) corroded rebars after cleaning.

to simulate the corrosion process in an accelerated manner in the laboratory. The two methods were able to reproduce the corrosion of reinforcement in R.C. structures reasonably well, but the constant current method was found to give a better reproduction of the corrosion process than the constant voltage method [12].

The accelerated corrosion of RC samples was done by passing a constant current of 2A through the reinforcing bars connected to the anode of the D.C. power supplies while also connecting a stainless steel plate to the cathode. Then, the connected specimen is placed in a salt bath with 10% sodium chloride (NaCl) by water weight to simulate the corrosive environment. 5% sodium chloride by weight of the cement was added to the concrete mix during casting to improve the conductivity of the R.C. column during the accelerated corrosion process. The setup for the accelerated corrosion is shown in Fig. 4 below.

The duration for the expected mass loss was estimated using Faraday's 2nd law of electrolysis [44] as follows:

$$\Delta m = \left(\frac{M}{Z}\right) \left(\frac{Q}{F}\right) \tag{1}$$

where, Δm is the estimated mass loss (g), M is the molar mass of the iron (56 g/mol), Z is the ionic charge for iron (valence electron transferred per ion = 2), and F is the Faraday's constant (96,500 C/mol). Q is the total electric charge passed through the substance and is calculated from Eq. (2) below:

$$Q = \int_0^T I dt = IT \tag{2}$$

where I is the magnitude of the applied current (Ampere, A), T is the estimated time to achieve the desired corrosion (s). Combining Eqs. (1) and (2) together gives;

$$\Delta m = \frac{MIT}{ZF} \tag{3}$$

The above equation (Eq. (3)) gives an approximate estimate of the expected corrosion mass loss, which could be different from the actual corrosion mass loss obtained after the corrosion process. Hence, the corroded bars are taken out of the columns after testing by breaking the

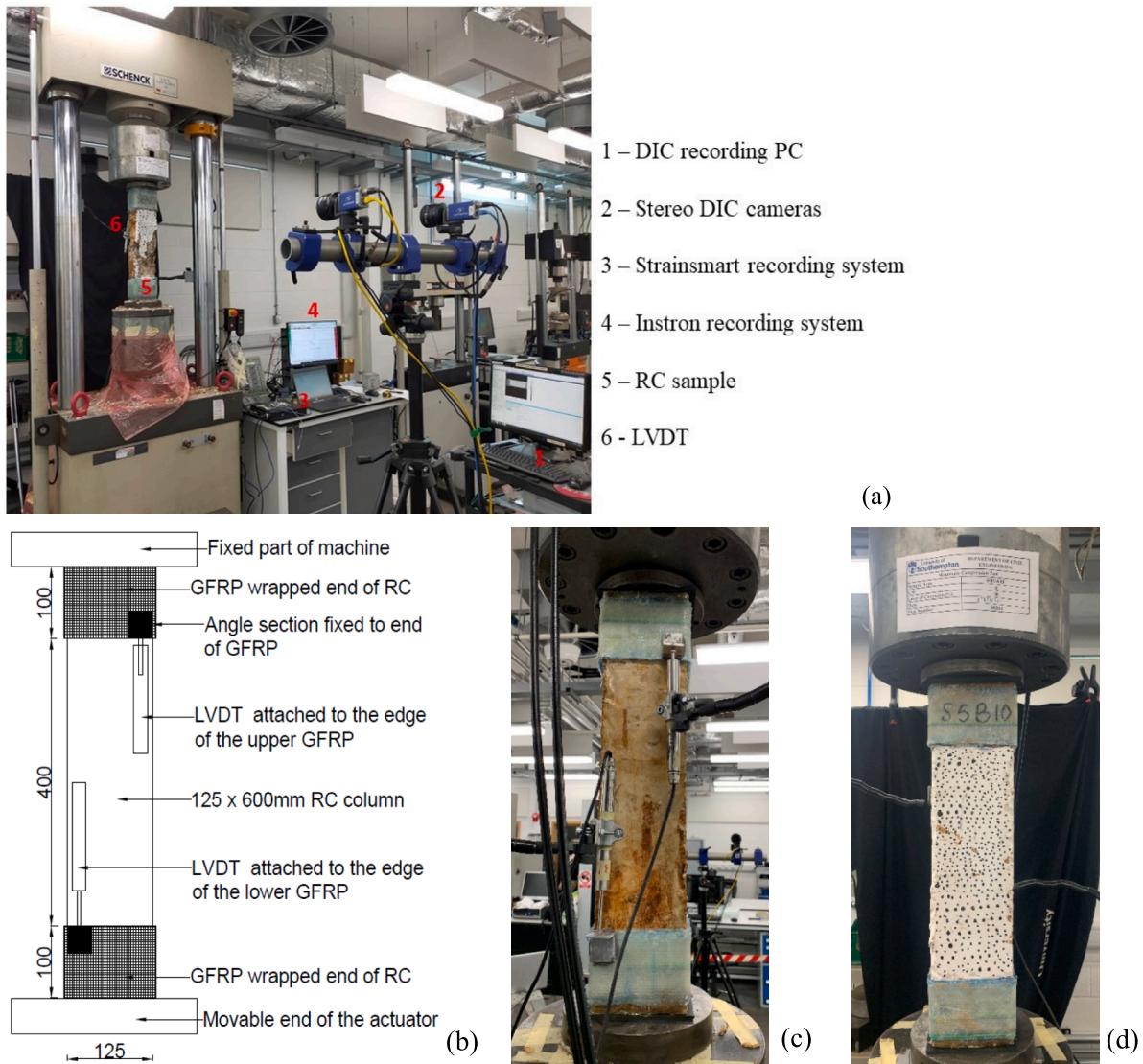


Fig. 5. Experimental test setup (a) laboratory setup; (b) schematic of the LVDT connection; (c) Image of the LVDT connections to the R.C. samples and (d) R.C. sample with speckles for DIC.

Table 4
 Corrosion properties of circular columns.

Specimen No.	Corrosion current density (mA/cm ²)	Corrosion duration (days)	Estimated mass loss (Eq. (3)) (%)	Measured mass loss of longitudinal bars (Eq. (4)) (%)	Measured mass loss of transverse bars (Eq. (4)) (%)
C5B0	0	0	0	0	0
C5B5	1.00	3.0	5	4.1	8.8
C5B10	1.00	6.0	10	7.3	21.2
C5B20	1.00	12.1	20	10.8	29.4
C5B30	1.00	18.1	30	20.6	39.8
C8B0	0	0	0	0	0
C8B5	1.16	2.7	5	4.9	13.0
C8B10	1.16	5.4	10	9.4	21.8
C8B20	1.16	10.8	20	16.5	41.4
C8B30	1.16	16.2	30	20.9	59.6
C13B0	0	0	0	0	0
C13B5	1.28	2.5	5	6.0	12.7
C13B10	1.28	5.0	10	12.5	30.1
C13B20	1.28	10.0	20	16.1	37.2
C13B30	1.28	15.0	30	27.6	45.9

Table 5
Corrosion properties of square columns.

Specimen No.	Corrosion current density (mA/cm ²)	Corrosion duration (days)	Estimated mass loss (Eq. (3)) (%)	Measured mass loss of longitudinal bars (Eq. (4)) (%)	Measured mass loss of transverse bars (Eq. (4)) (%)
S5B0	0	0	0	0	0
S5B5	0.99	2.9	5	3.4	10.9
S5B10	0.99	5.8	10	6.8	17.1
S5B20	0.99	11.7	20	13.8	37.0
S5B30	0.99	17.5	30	18.4	46.3
S8B0	0	0	0	0	0
S8B5	1.17	2.6	5	4.7	13.4
S8B10	1.17	5.1	10	9.8	18.9
S8B20	1.17	10.2	20	16.7	39.4
S8B30	1.17	15.3	30	24.8	53.3
S13B0	0	0	0	0	0
S13B5	1.33	2.3	5	6.2	11.8
S13B10	1.33	4.6	10	8.8	17.4
S13B20	1.33	9.3	20	10.7	25.3
S13B30	1.33	13.9	30	20.2	30.3

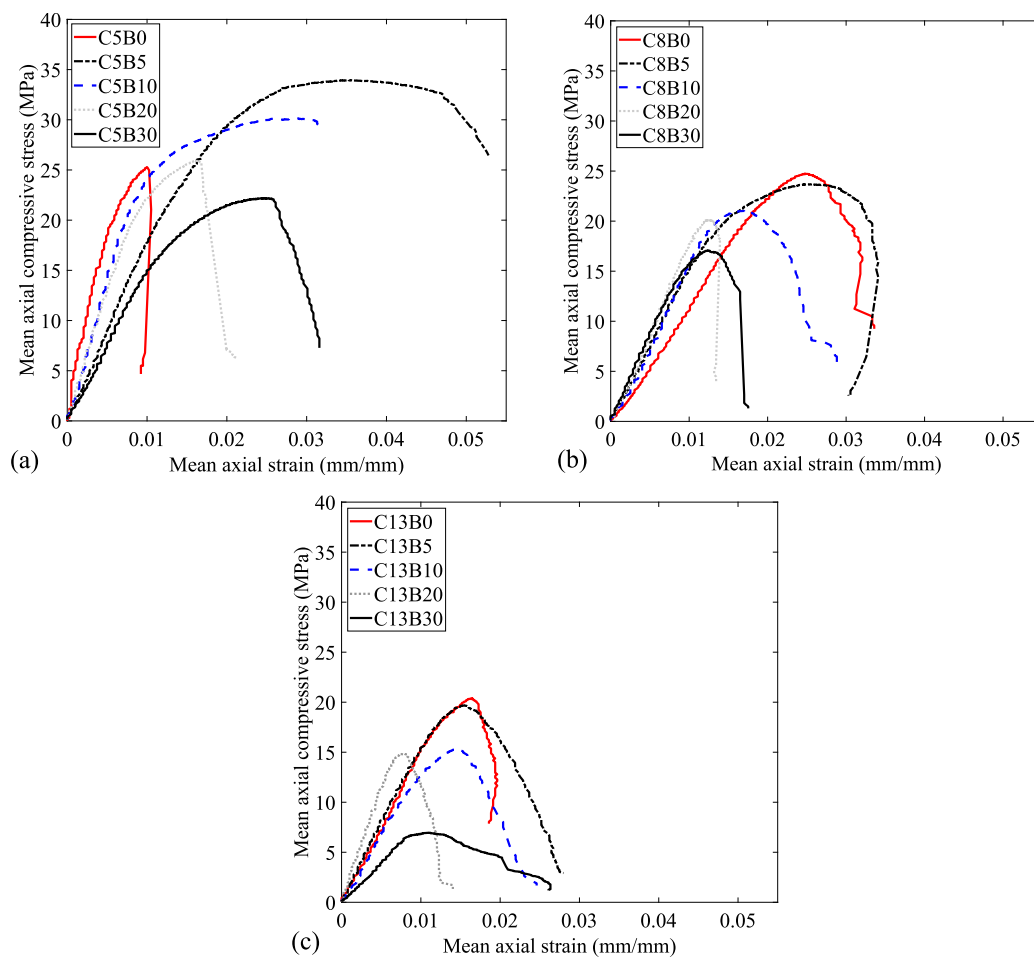


Fig. 6. Compressive stress–strain responses of the circular columns (a) L/D = 5, (b) L/D = 8 and (c) L/D = 13.

R.C. column. Then, the rebars were soaked in vinegar and cleaned with water and a wire brush to remove the surface’s concrete and rust particles per ASTM G1-03 [47]. This brushing and cleaning procedure was also applied to the uncorroded specimen, and the cleaning effect was negligible on the base materials [44]. Afterwards, the actual mass loss due to corrosion is estimated by weighing the rebars and is estimated from Eq. (4):

$$\gamma = \frac{m_0 - m}{m} \times 100 \tag{4}$$

where m_0 , is the mass per unit length of the uncorroded rebar, and m is the mass per unit length of the rebar after cleaning. This equation gives an average corrosion loss (mass loss) along the length of the rebar. It should be noted that there were not any disconnections between the stirrups and longitudinal reinforcement, and hence, the current applied to all the reinforcement.

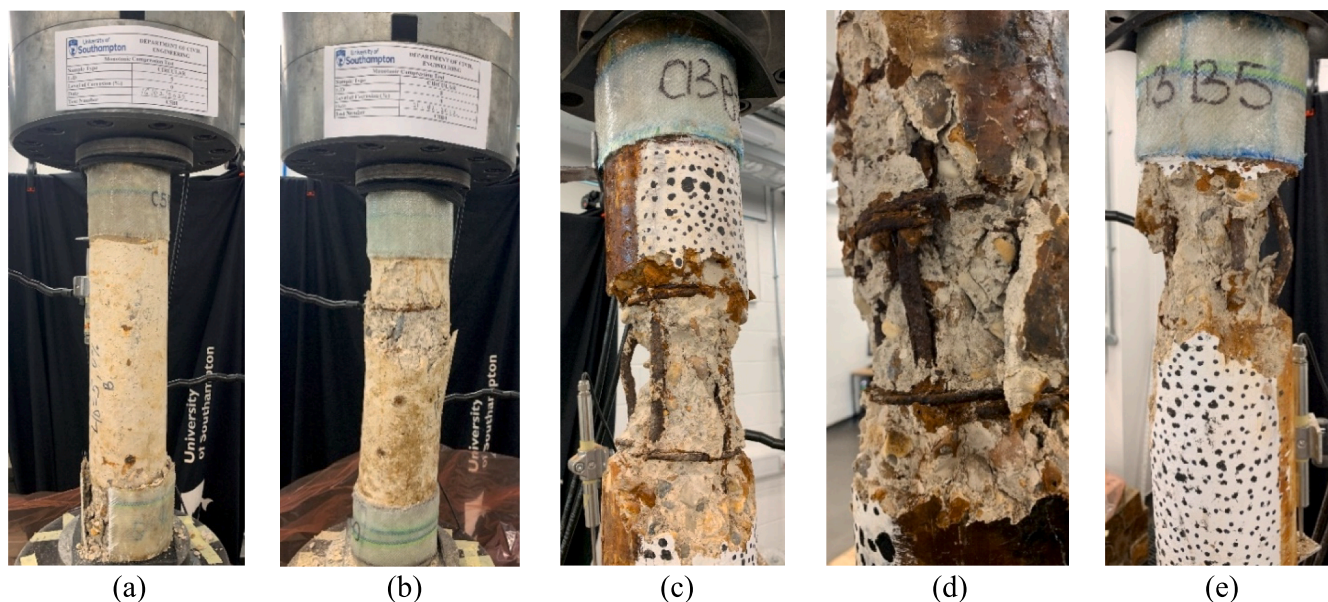


Fig. 7. Observed failure modes of circular columns. (a) GFRP failure; (b) spalling of concrete cover; (c) rebar buckling at middle zone; (d) transverse bar fracture, and (e) buckling of longitudinal bars below the GFRP.

3.3. Axial load testing and instrumentation

This experiment studied the response of R.C. columns under axial monotonic compressive loading using the 630 kN capacity Instron Schenck machine having a 250 mm travel. The machine used an internal Linear Variable Differential Transformer (LVDT) that measured the displacement of the actuator during loading. The test was conducted at a constant loading rate of 1 mm/min using the displacement control settings in the Instron Bluehill software. The setup of the experiment is shown in Fig. 5.

The displacement is measured with the LVDT, fixed to measure the displacement at the 400 mm middle zone of the R.C. columns, and the stereo 3D Digital Image Correlation (DIC). The two LVDTs with 50 mm stroke were clamped diagonally on the machine frame using magnetic robotic arms. They are fixed such that they touch the angle irons fixed to the edge of the Glass fibre-reinforced polymers (GFRP) strengthened ends of the R.C. columns (Fig. 5(b) and (c)). The LVDTs can thus measure the axial deformations in the middle 400 mm section of the columns. The displacements from the LVDTs are recorded via a multichannel data acquisition unit (Strainsmart 8000).

In addition, a digital image correlation (DIC) was performed, which is a non-destructive non-contact full-field optical measurement technique capable of capturing digital images of the surface of an object to obtain the in-plane strains and out-of-plane deformations in its 2D and 3D configurations. The DIC technique was deployed to capture the crack propagation and deformations on the R.C. columns under compressive load. The video imaging was performed using LaVision's Davis imaging software involving two cameras (Imager E-Lite 5 M) fitted with Nikon AF Nikkor 28 mm f/2.8D (28 mm focal length and 2.8 maximum aperture) lenses. The cameras were calibrated to capture the R.C. column's out-of-plane and vertical displacements during loading using the dots marked on the columns (Fig. 5(d)). The images recorded are further processed using LaVision's Davis 10 software to see the strain distribution.

4. Experimental test results and discussions

4.1. Calculation of corrosion and mass loss ratio

The actual mass loss resulting from the corrosion of the

reinforcements is estimated using Eq. (4). The results for the mass loss are illustrated in Tables 4 and 5 for the circular and square columns, respectively. The results indicate that the transverse stirrups had more severe corrosion than the longitudinal bar under the same constant current and duration [48]. This results from the closeness of the transverse bars to the surface of the concrete, leading to a possibly higher concentration of chloride ions and an early start of corrosion [49]. Furthermore, the diameter of the longitudinal rebar (10 mm) were greater than that of the stirrups (6 mm). In this regard, the mass loss ratio of transverse stirrups with smaller diameters was higher than that of the longitudinal rebar, according to Faraday's second law of electrolysis [44].

The localised corrosion of reinforcements results from applying a higher current at a shorter duration during the corrosion of rebars [50]. Hence to obtain more general and uniform corrosion, a low current is recommended at a shorter duration as the application of low current at a longer duration also results in localised corrosion [50]. In this work, a constant current of 2A was used for the accelerated corrosion of the R.C. columns. This results in corrosion current densities in Tables 4 and 5, with the square columns having higher corrosion densities in the sparsely confined columns than the circular columns with similar configurations. Furthermore, the applied current density is close to the 1 mA/cm² recommended by Nguyen [50] for the laboratory simulation of corrosion of steel embedded in concrete.

4.2. Axial load testing of circular columns

The stress–strain response of the circular column to the applied axial compressive load is presented in Fig. 6(a–c). It should be noted that the stress–strain response plotted was from the LVDTs data, as the readings from the load cell of the hydraulic machine were ignored since it captures the deformation of the whole sample instead of the required middle zone section. Similar behaviour was observed for all the R.C. column samples. Vertical minor cracks first developed on the concrete and, subsequently, became enlarged resulting in the crushing and spalling of the concrete cover as the longitudinal bars buckled due to lateral expansion of the R.C. column. The observed compressive response of the columns is similar at the elastic range until yield and afterwards reduces beyond the peak load due to corrosion and confinements of the rebars [51]. The axial load-carrying capacities of the

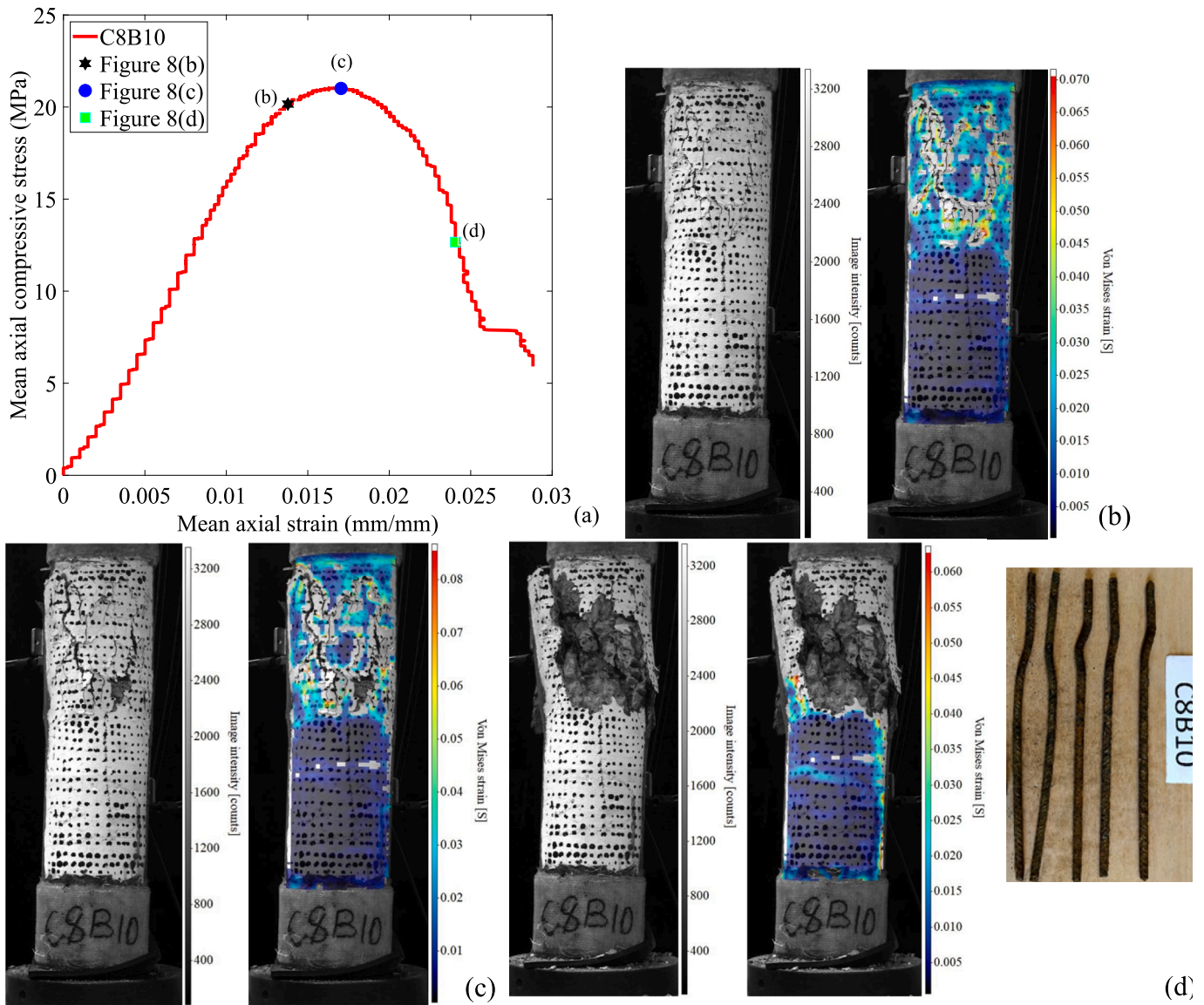


Fig. 8. Processed DIC images of a circular column (a) stress–strain response showing location of processed images (b) at yield stress, (c) at ultimate stress and (d) between ultimate stress and collapse.

columns generally decrease within each configuration of columns, except in some cases where the control sample (0% corrosion) recorded low capacity due to the premature failure of the strengthening GFRP at the top/bottom of the column (Fig. 7(a)). Also, the applied axial load results in the concrete cover spalling (Fig. 7(b)), buckling of the longitudinal bar and, in some cases, fracture of the transverse and longitudinal bars (Fig. 7(d)). The observed buckling position of the column varies with the different confinement configurations, with the $L/D = 5$ and $L/D = 8$ confined columns generally failing by buckling at the middle zone. In contrast, in the sparsely confined samples ($L/D = 13$), the buckling occurs immediately below/above the GFRP zones (Fig. 7(e)).

The different in the initial stiffness is due to the impact of confinement and inelastic buckling. The concrete is low-strength, and hence, its compressive behaviour is significantly affected by confinement reinforcement ratio. Furthermore, the concrete does not provide any lateral restraint against buckling. Therefore, vertical bars are restrained against buckling by the transverse tie reinforcement. As a result, the concrete in test specimens with larger transverse tie spacing starts crushing followed by buckling of vertical bars much earlier than the columns with more

confinement ratio; i.e. closer transverse tie spacing. This has a significant impact on the initial stiffness of tests specimens.

The corrosion mass loss of both the longitudinal and transverse bars results in the reduction of the ultimate strength and load-carrying capacity of the column. Consequently, columns with very similar mass loss have their maximum strength quite close to each other. This trend is observed in all the different column configurations with an estimated mass loss between 10% and 20% (Fig. 6(a–c)).

The DIC tracks the R.C. columns' strain response and cracks damage to the applied compressive load. Fig. 8(a) shows the stress–strain response of one of the circular columns and the locations of the processed images (at yield stress, ultimate stress and beyond the ultimate stress). The processed images within the column's middle zone section showed the column's strain contour with the cracks, spalling of the cover concrete, and the buckling of the reinforcement captured. Fig. 8 (b–d) show the processed images with the Von Mises strain. These values correspond to the strain estimated from the LVDTs at yield stress, ultimate stress and beyond the ultimate stress.

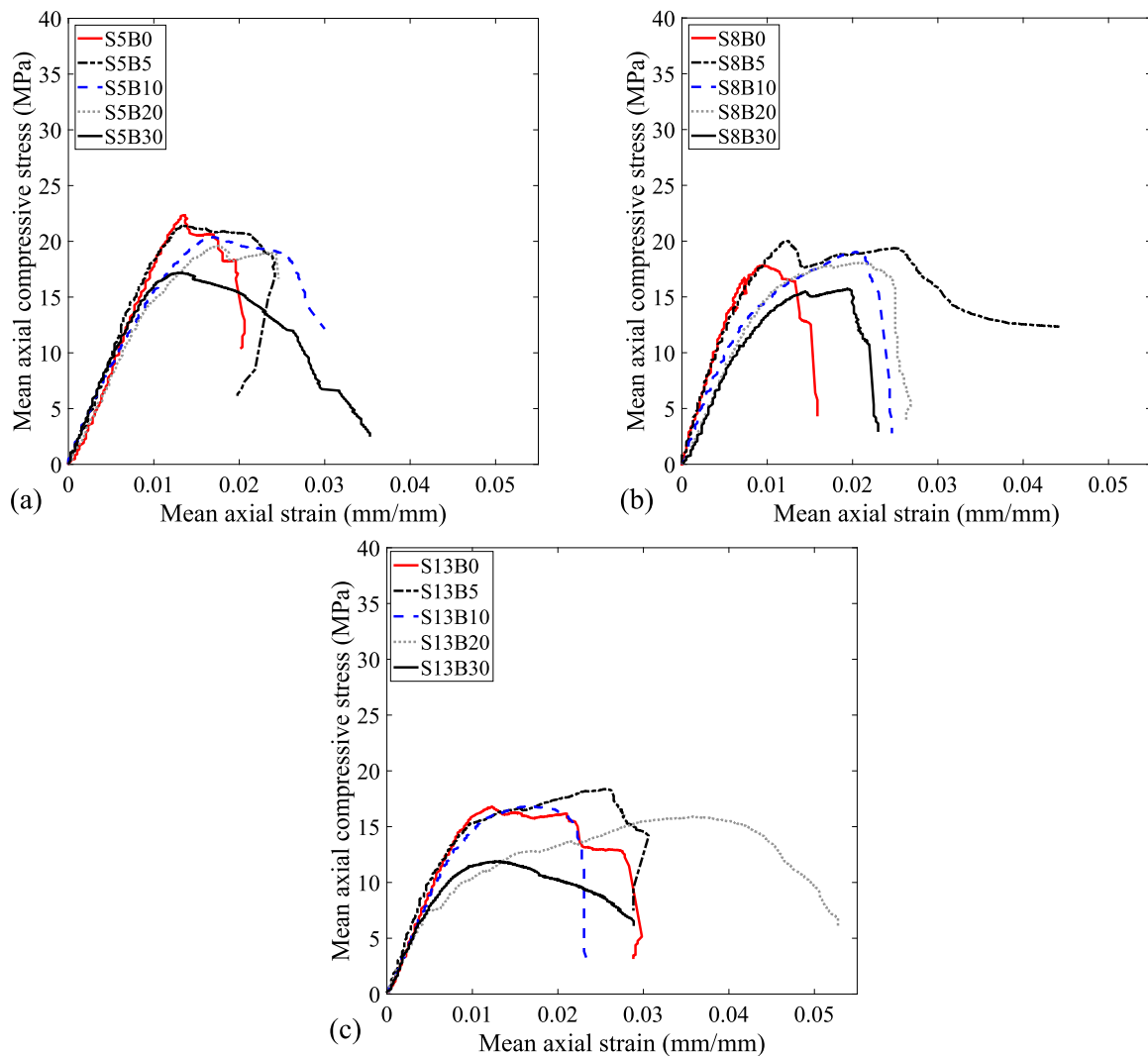


Fig. 9. Axial compressive stress–strain responses of square columns (a) $L/D = 5$, (b) $L/D = 8$ and (c) $L/D = 13$.

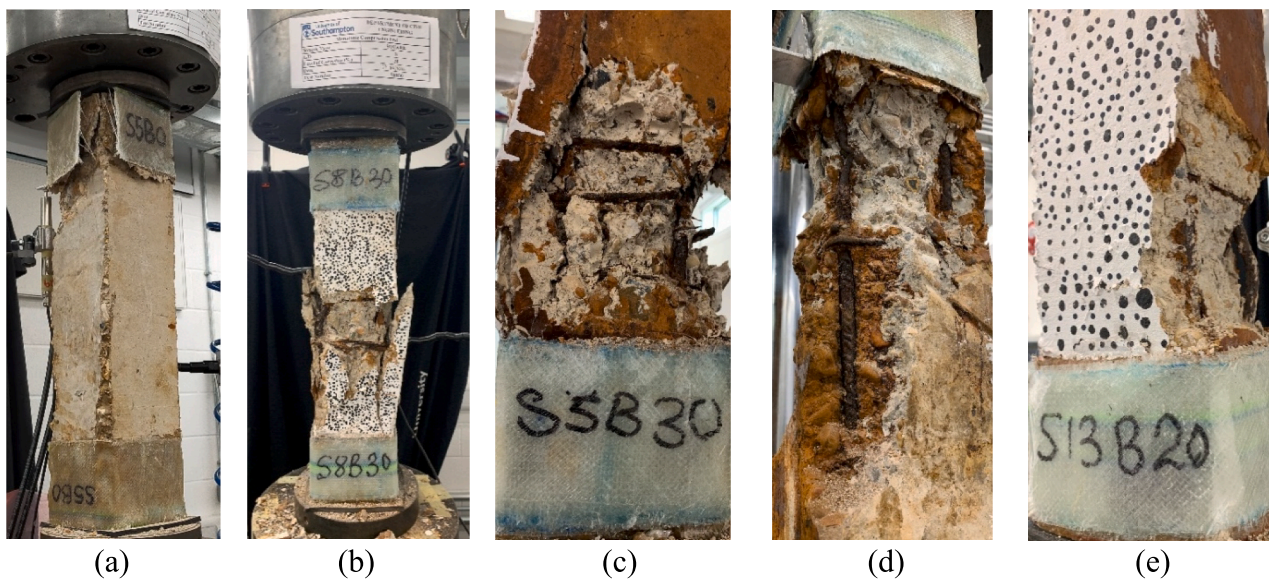


Fig. 10. Observed failure modes of the square columns. (a) GFRP failure at the top; (b) spalling of concrete cover; (c) transverse bar fracture; (d) longitudinal bar fracture at pitting corrosion location and (e) buckling of longitudinal bars above the GFRP.

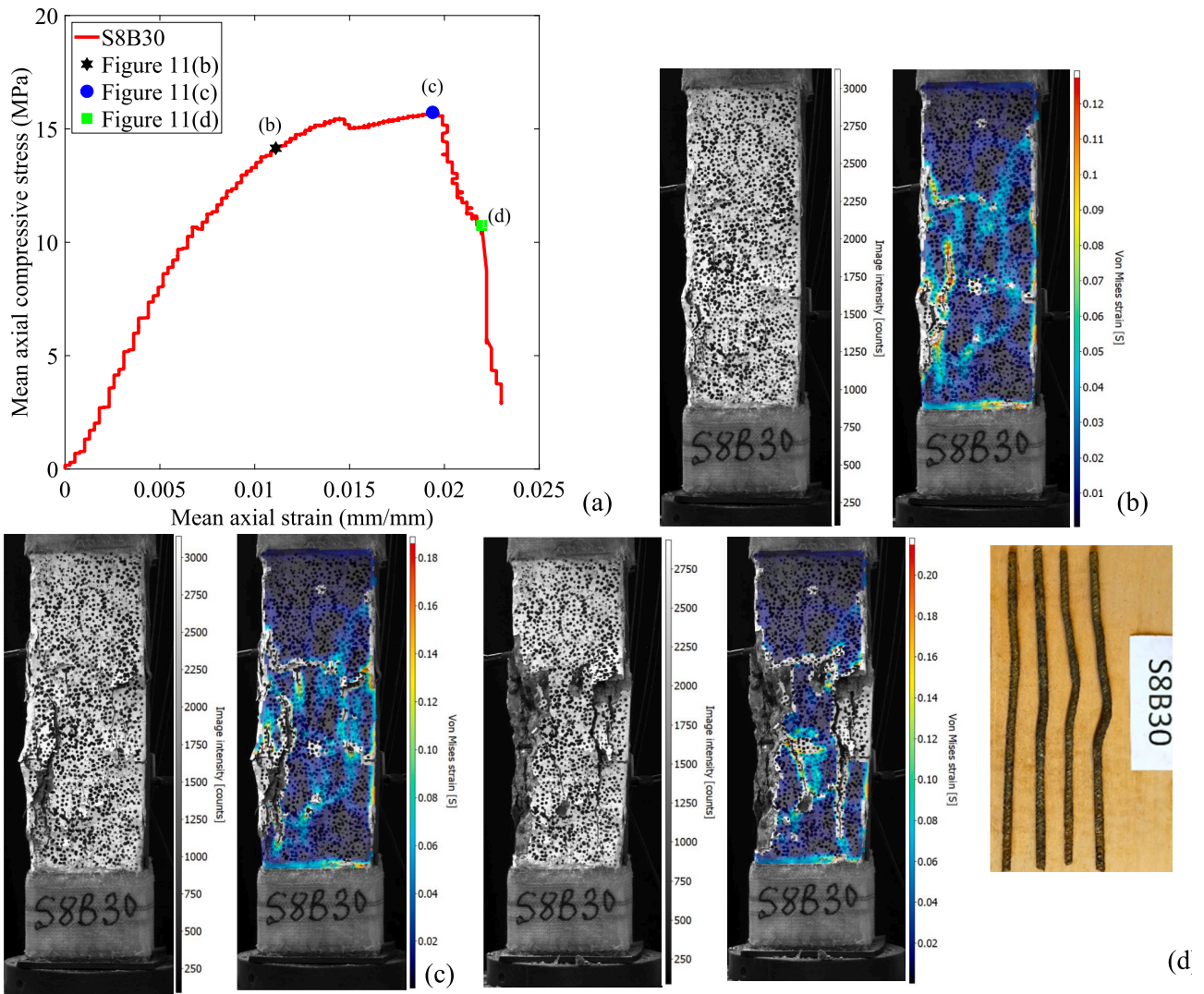


Fig. 11. Processed DIC images of a square column (a) stress–strain response showing location of processed images (b) at yield stress, (c) at ultimate stress and (d) between ultimate stress and collapse with the buckling at the end of the test.

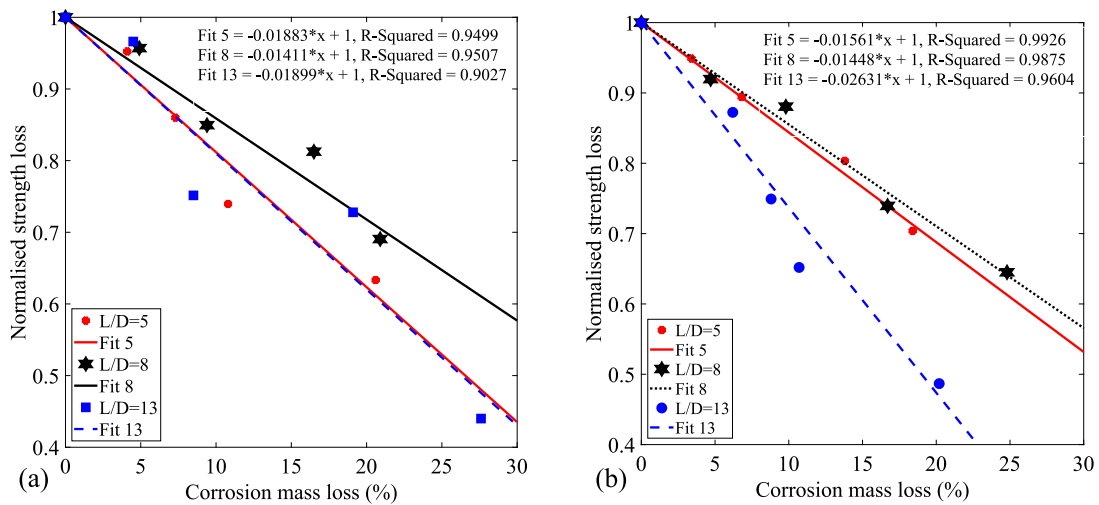


Fig. 12. Strength variation of the confined R.C. columns with corrosion (a) circular and (b) square.



Fig. 13. Observed buckling failure of the longitudinal reinforcement after testing; L/D = 5 (a–d), L/D = 8 (e–h) and L/D = 13 (i–l).

4.3. Axial load testing of square columns

The stress–strain response of the square columns to the applied axial compressive load is similar to the behaviour of the circular columns and is presented in Fig. 9(a–c). The more closely confined columns (L/D = 5) have higher load-carrying capacities, which reduces with an increase in corrosion mass loss. Also, some of the control samples (0% corrosion) recorded low capacities (Fig. 9(b) and (c)) resulting from the failure of the strengthening GFRP at the top/bottom of the column (Fig. 10(a)), leading to stress concentration and premature failure of the ends of the columns. The failure of the GFRPs occurs due to the sharp edges of the columns.

Similar to the circular columns, the applied axial load results in the concrete cover's spalling, transverse bars fracture and longitudinal bars buckling. The stress–strain relationship shows similar behaviour within the elastic region in all the columns until the yield stress, beyond which the confinement configurations and increase in the corrosion degree results in a subsequent decrease in the axial load-carrying capacities.

Fig. 11(a) shows the stress–strain response of one of the square columns with an estimated 30% corrosion mass loss. Fig. 11(b–d) are the processed images from the DIC at different locations during the compression test on the column. The processed images within the middle zone section of the column showed the images with and without the strain contour on the column with the crack propagation, spalling of the cover concrete and the reinforcement's buckling. Fig. 11(d) further shows the buckled longitudinal bar after removal and cleaning.

It is observed that the circular columns generally have better axial load-carrying capacities and axial strain than the square columns [30,52]. This results from the effectiveness of the transverse ties in the circular column, which has more significant confinement effectiveness coefficients than the square columns [30].

4.4. Impact of corrosion on the strength of confined R.C. Column

The strength loss resulting from the corrosion and confinement ratios of the R.C. columns is determined by normalising the ultimate strength of the corroded columns to the ultimate strength of the uncorroded. The estimated maximum strength of the uncorroded column is used in the normalisation due to premature failure of the tested uncorroded column. The ultimate strength is estimated from Eq. (5).

$$\sigma_u = \frac{\sigma_c(A_g - nA_s) + nA_s\sigma_s}{A_g} \quad (5)$$

where, σ_c is the compressive strength of unreinforced concrete in MPa, A_g is the cross-sectional area of the R.C. column in mm^2 , n is the number of longitudinal rebars, A_s is the area of longitudinal rebar in mm^2 and σ_s is the ultimate strength of the rebar in MPa.

The normalised ultimate strength loss of the different confined R.C. columns is plotted relative to the percentage of corrosion mass loss. Linear trend lines are fitted to the test data to estimate the strength reduction due to corrosion and confinement ratios. The R-square goodness of fit values obtained from the trend lines range from 0.95 to 0.90 for the circular columns at different confinement ratios (Fig. 12a), while the variation for the square columns is from 0.99 to 0.96 (Fig. 12b).

The ultimate strength of the confined corroded R.C. columns is reduced with an increase in the confinement degree and corrosion mass loss. For example, the well-confined circular columns with L/D = 5 (Fig. 12(a)) have a strength reduction range of 4.7%, 14%, 26% and 36.7% for the 4.1%, 7.3%, 10.8% and 20.6% corrosion mass loss, respectively. Also, the well-confined square columns with L/D = 5 (Fig. 12(b)) have a strength reduction range of 5.1%, 10.6%, 19.6% and 29.6% for the 3.4%, 6.8%, 13.8% and 18.4% corrosion mass loss, respectively. A similar trend is also observed in the mediumly confined (L/D = 8) and sparsely confined (L/D = 13) columns, with the strength reduction increasing with an increase in the corrosion mass losses in the circular and square columns.

4.5. Impact of corrosion on inelastic buckling behaviour of vertical reinforcement

Corrosion generally reduces the cross-sectional areas of bars available to sustain the applied load [53]. This reduction becomes more severe in bars with pitting corrosion, resulting in localised reduction in the cross-sectional areas of the bars, leading to rebar fracture and localised buckling (Fig. 13). The results of the tests on the corroded columns showed that the pitting effect is more significant, as it leads to the buckling mechanism and reduction in the load-carrying capacity of the column. Longitudinal bars in columns with L/D = 5 confinement had less buckling failure, especially at lower corrosion than bars from the L/D = 8 and L/D = 13 configurations [44,53]. This buckling from the columns with L/D = 5 rebars at higher corrosion levels results from the unsymmetrical cross-sections arising from the pitting corrosion causing imperfections in the bar and leading to additional bending moment and local stresses at the pitted sections [44,54]. Meanwhile, the buckling from the columns with L/D = 8 and L/D = 13 results from the combination of pitting corrosion and inadequate confinement provisions leading to premature yielding and squashing of the weakest section even at lower corrosion degrees [55]. Those columns with more uniformly distributed corrosion and a relatively small mass loss showed similar behaviour to those with uncorroded bars with a more visible buckling at higher compressive load [44].

5. Comparison of the response of circular and square columns

Fig. 14(a–l) shows the normalised stress–strain response of the circular and square columns with similar confinement configurations and

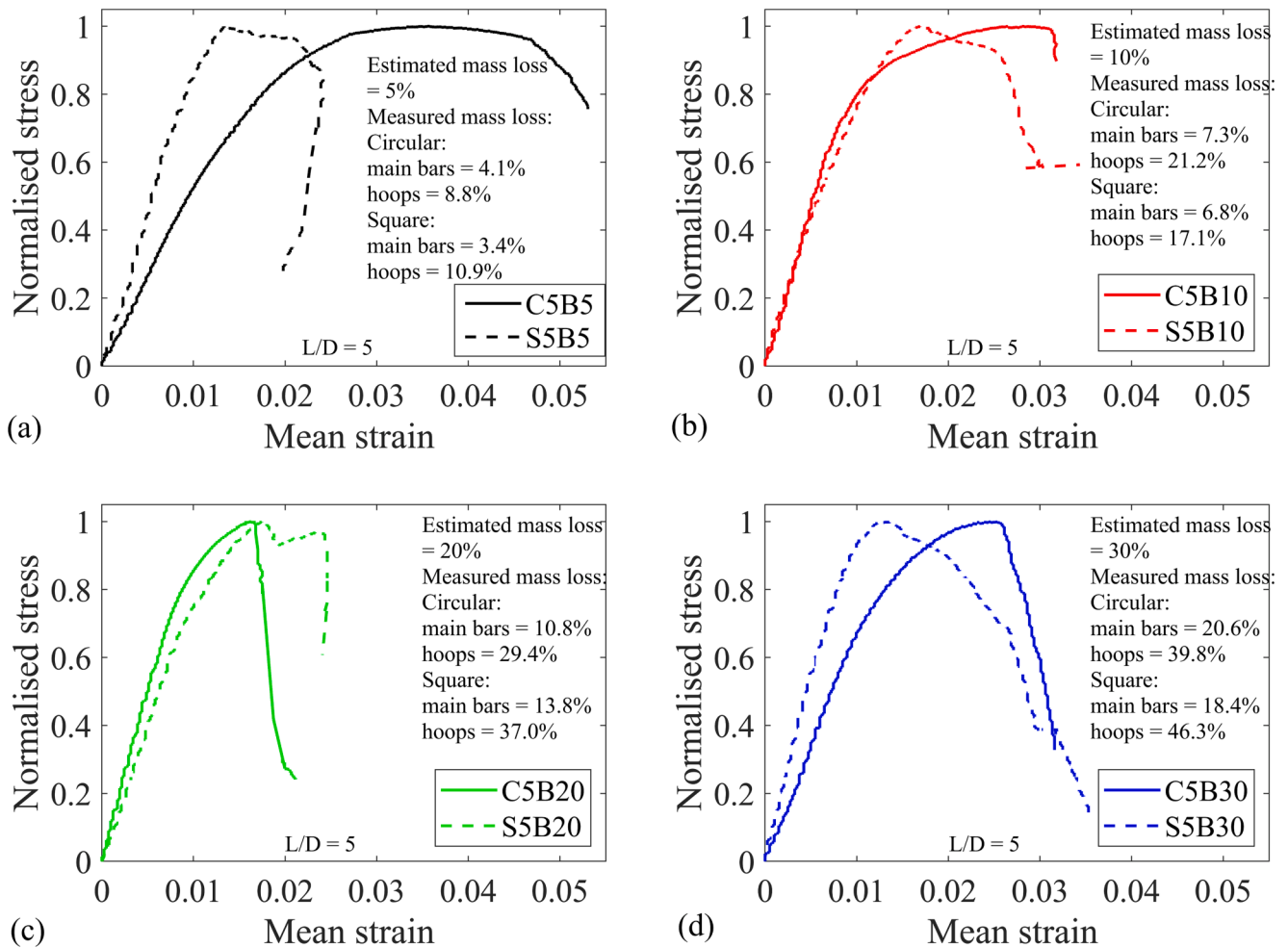


Fig. 14. Comparison of the normalised stress response of circular and square columns with varying corrosion and confinement levels; L/D = 5 (a–d), L/D = 8 (e–h) and L/D = 13 (i–l).

corrosion mass losses. First, the ultimate strength of the columns is normalised and plotted against the corresponding strain values. The columns show similar responses and stiffness within the elastic region until the peak strength is attained. Afterwards, the corrosion and confinement results in a loss of stiffness and reduced ductility of the R.C. columns. Generally, the highly confined columns ($L/D = 5$) with smaller corrosion mass loss have a higher ductility (especially the circular columns) than columns in the mediumly confined ($L/D = 8$) and lowly confined ($L/D = 13$) at the same corrosion levels. This behaviour is observed to be the same in the columns within the same configurations as the corrosion level increases.

Furthermore, the columns' ductility reduced with an increase in the confinement levels in all the columns. This behaviour is also similar to the corrosion mass losses, where an increase in the corrosion loss results in a decrease in the ductility of the column in almost all the different confinement configurations.

6. Comparison of existing analytical models with experimental results

Various models have been proposed to investigate the stress–strain response of confined concrete. These analytical models were developed from observations in experimental studies with several adjustments to account for the confinement of the concrete core. Mander et al. [27] unified stress–strain model, which is based on the multiaxial properties of concrete, is the most popular confined concrete model. The model

defined an effective lateral confining stress dependent on the transverse and longitudinal bars. Despite its popularity, the model does not include the effect of reinforcement corrosion, resulting in its inapplicability for corroded R.C. structures.

Several researchers have used analytically developed stress–strain graphs of confined concrete subjected to corrosion for numerical applications without experimental verification [33,34] (Ou et al. 2013; Ou and Nguyen 2014). For example, Coronelli and Gambarova [56] validated their numerical model through comparison with available test data on simply-supported beams. Still, the analytically proposed stress–strain model of confined concrete used in their numerical simulation was not experimentally validated.

In this work, three existing stress–strain models on corroded R.C. columns with varying degrees of corrosion and different column configurations were compared with the experimental results. The models adopted [4,10,31,32] modified the one from Mander et al. [27] to reflect the effect of corrosion on the strength of confined concrete by adjusting the yield strengths of the transverse reinforcement. The expressions of the existing models are shown in Tables 5 and 6. All of the proposed models considered the effect of corroded transverse reinforcement on the peak strength and the ultimate strain without considering the effect of the corrosion of the longitudinal rebar. The models show a satisfying performance in predicting the ultimate condition of the corroded R.C. columns with different degrees of corrosion of the stirrup [57].

To compare the experimental data with this models, the ultimate strength from the test is adjusted by removing the stress resulting from

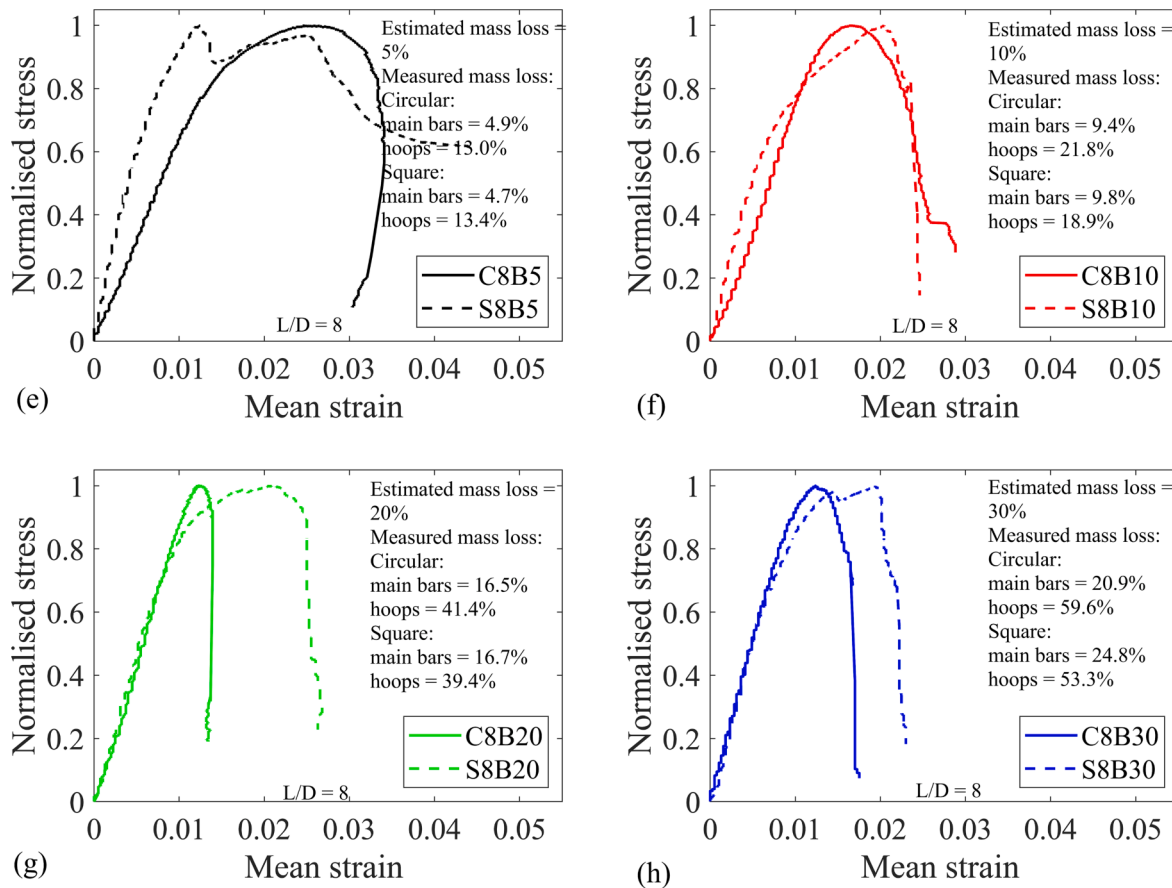


Fig. 14. (continued).

the longitudinal bars from the ultimate strength of the R.C. Hence, the strength of confined concrete is estimated from Eq. (6).

$$\sigma_c = \frac{(\sigma_g \times A_g) - nA_s \sigma'_{yc}}{A_g - nA_s} \quad (6)$$

The yield strength of the longitudinal bar is adjusted to reflect the corrosion and buckling effect using the equation proposed by Kashani et al. [44].

$$\sigma'_{yc} = \sigma_y (1 - \beta \gamma) \quad (7)$$

where, σ'_{yc} , is the yield stress of corroded bars in compression, $\beta = 0.005$ for $L/D \leq 5$, $\beta = 0.0065$ for $5 < L/D \leq 10$, $\beta = 0.0125$ for $L/D > 10$ and γ , is the corrosion mass loss determined in Eq. (4).

Fig. 15 shows the performance of the selected existing analytical models in predicting the compressive strength of confined corroded R.C. columns. It can be seen from the comparison that the current analytical models overestimate the peak strength of the confined columns. This is because the ultimate strength of confined concrete columns depends on the strength of the unconfined concrete, the dimensions of the core and the amount and configuration of transverse reinforcements. Thus, the observation of higher ultimate strength arising from the analytical models in comparison to the experimental data results from the low compressive strength of the concrete used in the experimental tests. Furthermore, the response of confined concrete columns to lateral pressure is affected by changes in the cross sections. Hence, columns with circular cross-sections have higher strength capacity, which is about double that of the square cross-sections when subjected to the same lateral confining pressure. This differences in the lateral confining pressures results from the irregularity in the distribution of pressure in the cross-section of the square columns. In addition, the strength

predictions for the square columns are within the variability of the experimental data.

7. Conclusion

The effects of corrosion on the axial load capacity of differently confined R.C. columns have been studied experimentally. The parameters investigated in this study are corrosion mass loss on the stress–strain response of differently confined circular and square R.C. columns representing typical shapes of bridge piers. The experiments were performed on 30 short R.C. columns divided into two groups of fifteen circulars and fifteen squares, subdivided into five groups according to the expected corrosion mass loss from the accelerated corrosion process and three groups considering the spacing of their transverse confining rebars. The Primary conclusions drawn from the analysis of the experimental data are as follows.

Corrosion of reinforcements severely weakens the load-carrying capacity, stiffness and ductility of reinforced concrete columns. In addition, corroded specimens fail due to fractures of stirrups at corners and buckling of longitudinal reinforcements. Furthermore, chloride corrosion causes severe pitting of the rebar and reduces the column's yield strength and load-carrying capacity.

The degree of corrosion experienced by transverse reinforcement is more severe than longitudinal reinforcements at the same current densities. This results from the closeness of the transverse bars to the surface of the concrete, leading to a possibly higher concentration of chloride ions and an early start of corrosion of the transverse bars.

Local buckling is more severe for specimens with high corrosion rates, and buckling always occurs in areas with more rust products. This is evidence that the local buckling of the rebar is strongly related to its corrosion condition, and the part where the cross-sectional area is

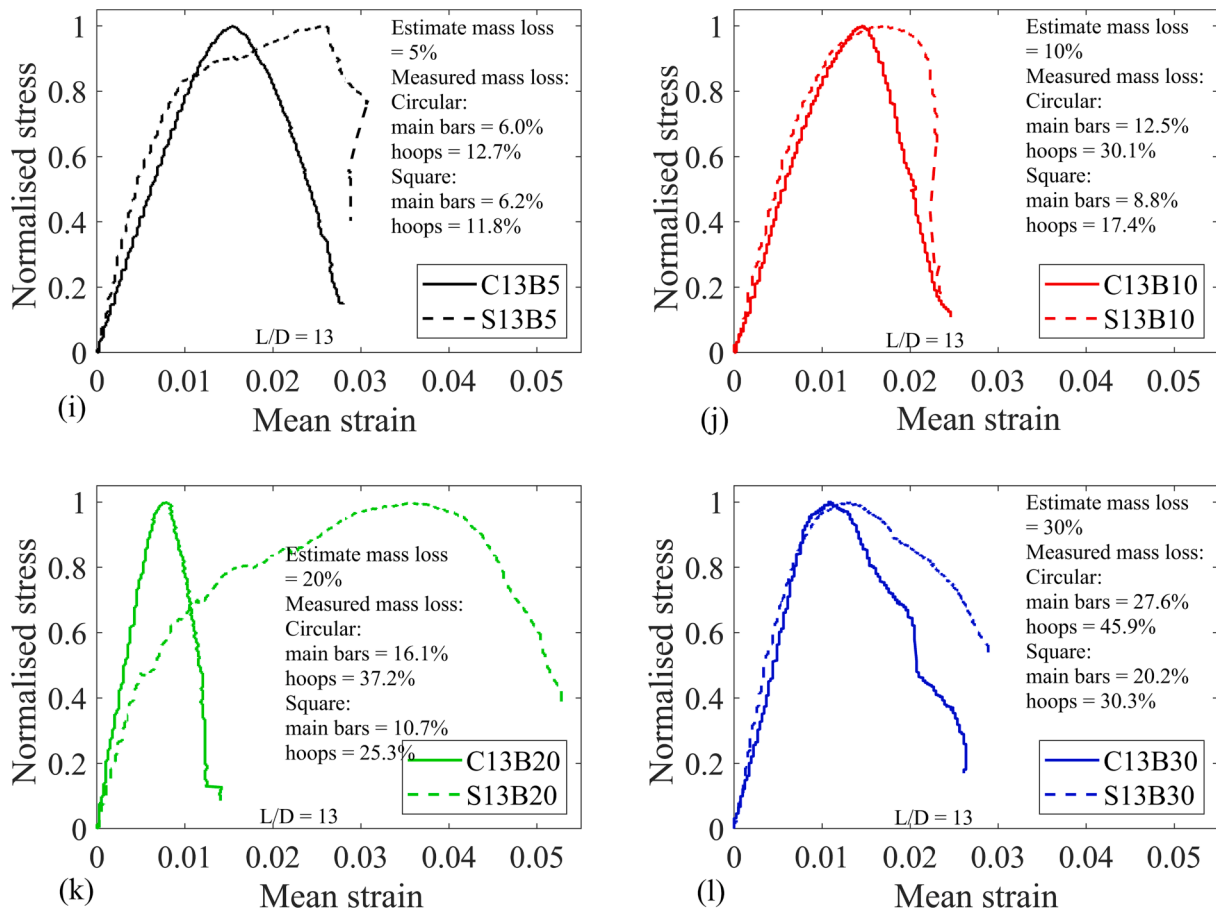


Fig. 14. (continued).

Table 6
Ultimate strength and strain of analytical models.

Model	Ultimate strength	Ultimate strain	Column type
Vu et al. [4]	$\sigma_{cc} = (1 - \alpha X_{corr}) \cdot \sigma'_{co} \cdot (-1.254 + 2.254 \cdot \sqrt{1 + (\frac{7.94f'_l}{\sigma'_{co}}) - 2 \cdot \frac{f'_l}{\sigma'_{co}}}) \alpha = 0.51$	$\epsilon'_{cu} = 0.004 + (1 - X_{corr}) \cdot \frac{2.8\epsilon'_{sm}f'_l}{fcc}$	Square and circular
Hoshikuma et al. [31]	$\sigma_{cc} = \sigma_{co}(1.0 + 3.8\alpha \frac{\rho_s f_{yh}}{f_{co}}) \alpha = 1.0$ and 0.2 for circular and square sections	$\epsilon'_{sm} = (1 - \tau X_{corr}) \epsilon_{sm}$ $\epsilon'_{cu} = 0.002 + 0.033\beta \frac{\rho_s f_{yh}}{\sigma_{co}}$ $\beta = 1.0$ and 0.4 for circular and square sections	Square and circular
Ma et al. [10]	$\sigma'_{cc} = \sigma'_{co}(-1.6 + 2.6 \sqrt{1 + (\frac{10f'_l}{\sigma'_{co}}) - 2 \cdot \frac{f'_l}{\sigma'_{co}}})$	$\epsilon'_{cu} = 0.004 + (1 - 0.559X_{corr}) \frac{0.216\beta_{xy}\rho_{sc}f_{yh}\epsilon_{sm}}{\sigma'_{cc}}$	rectangular
Andisheh et al. [32]	$\sigma'_{cc} = \sigma'_{co} \left(2.254 \sqrt{1 + (\frac{7.94f'_l}{\sigma'_{co}}) - 2 \cdot \frac{f'_l}{\sigma'_{co}}} - 1.254 \right)$	$\epsilon'_{cu} = 0.004 + (\frac{1.4\rho_s f_{yh} \epsilon'_{su}}{\sigma'_{cc}})$	Circular

α , is the stress correction coefficient; ϵ'_{sm} , is the steel strains at the maximum tensile stress of corroded transverse reinforcement; ϵ_{sm} , is the ultimate strain of uncorroded transverse reinforcement; τ , is the reduction factor for the ultimate strain of uncorroded reinforcement; f'_l , is the lateral confining pressure of the R.C. column; σ'_{co} , compressive strength of uncorroded reinforcement.

weakened by corrosion is more likely to cause buckling of the rebar. The inelastic buckling mechanism of bars is affected by non-uniform pitting corrosion. The observed buckling modes showed that the buckling mechanism of corroded bars is a function of the mass loss due to corrosion and the distribution of pits along the bar length. Hence, the bars with more corrosion mass loss experienced more buckling and fracture than columns at low corrosion. The existing analytical models overestimate the ultimate strength of low-strength confined corroded columns. Hence, there is a need for more experimental tests on low-strength concrete to develop a better analytical model that will correctly predict the strength of such R.C. columns.

CRedit authorship contribution statement

Hammed O. Aminulai: Writing the paper, conducting the experimental testing and data analysis. **A. F. Robinson:** Experimental officer supporting the first author in conducting the experimental testing. **Neil S. Ferguson:** Editing the paper and supervising the first author. **Mohammad M. Kashani:** lead supervisor, leading the research, supervising the student, and editing the paper.

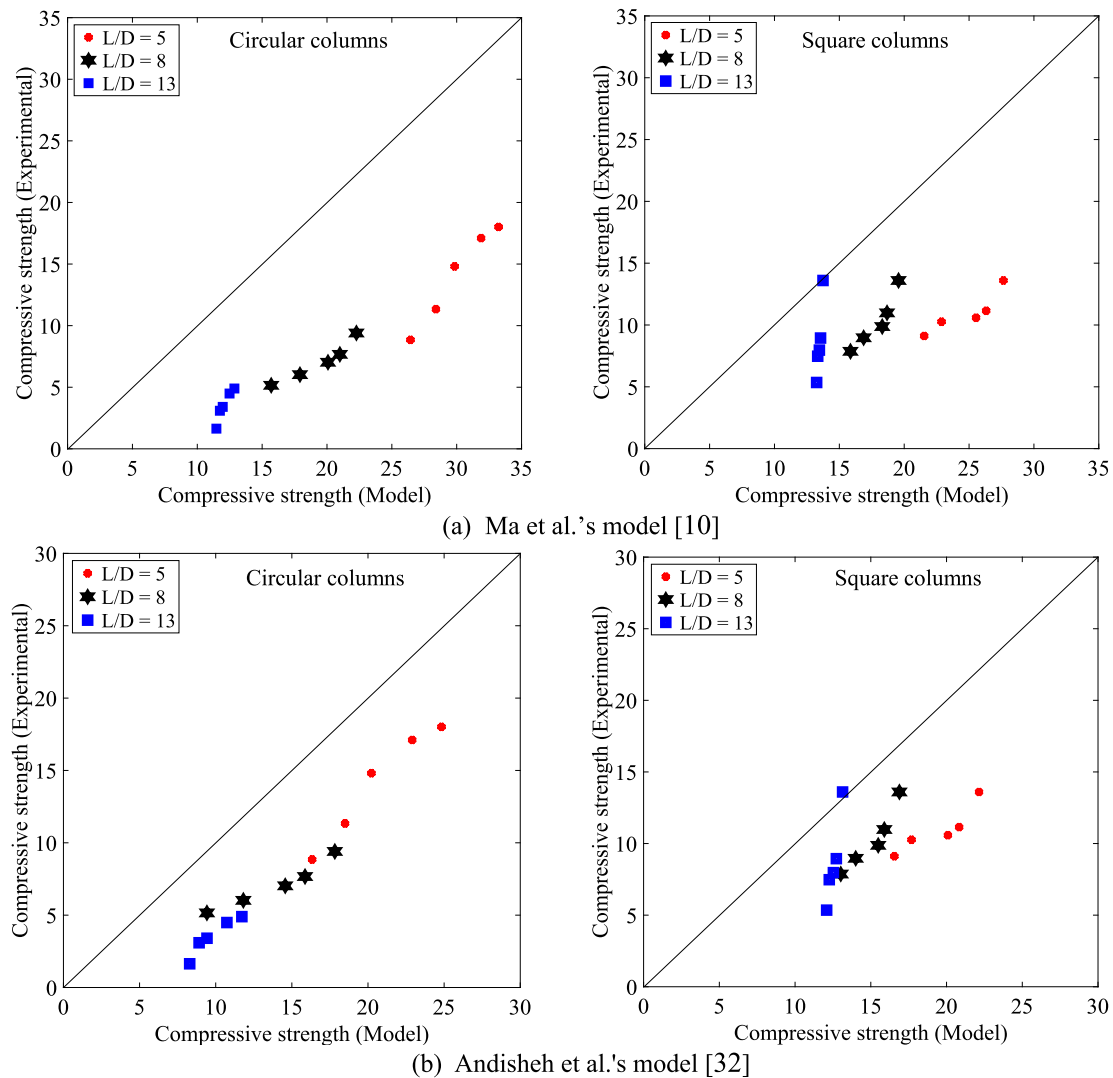


Fig. 15. Comparison of existing confined concrete models and experimental results of ultimate compressive strength.

Declaration of Competing Interest

The authors declare that they have no known competing financial interests or personal relationships that could have appeared to influence the work reported in this paper.

Data availability

Data will be made available on request.

References

- [1] S.T. Karapetrou, S.D. Fotopoulou, K.D. Ptilakisa, Seismic vulnerability of RC buildings under the effect of aging, *Procedia Environ. Sci.* 38 (2017) 461–468.
- [2] S.-Y. Yang, et al., Experimental research on hysteretic behaviors of corroded reinforced concrete columns with different maximum amounts of corrosion of rebar, *Constr. Build. Mater.* 121 (2016) 319–327.
- [3] M.M. Kashani, et al., Impact of corrosion on low-cycle fatigue degradation of reinforcing bars with the effect of inelastic buckling, *Int. J. Fatigue* 77 (2015) 174–185.
- [4] N.S. Vu, B. Yu, B. Li, Stress-strain model for confined concrete with corroded transverse reinforcement, *Eng. Struct.* 151 (2017) 472–487.
- [5] Y.G. Du, L.A. Clark, A.H.C. Chan, Residual capacity of corroded reinforcing bars, *Mag. Concr. Res.* 57 (3) (2005) 135–147.
- [6] N.S. Vu, L. Bing, Seismic performance assessment of corroded reinforced concrete short columns, *J. Struct. Eng.* 144 (04018018) (2018) 1–12.
- [7] C. Goksu, A. Ilki, Seismic behavior of reinforced concrete columns with corroded deformed reinforcing bars, *ACI Struct. J.* 113 (5) (2016) 1053–1064.
- [8] D. Shen, et al., Seismic performance of corroded reinforced concrete beam-column joints repaired with BFRP sheets, *Constr. Build. Mater.* 307 (2021), 124731.
- [9] X. Luo, et al., Seismic behavior of corroded reinforced concrete column joints under low-cyclic repeated loading, *Arch. Civil Mech. Eng.* 20 (2020) 40.
- [10] J. Ma, et al., Stress-strain model for confined concrete in rectangular columns with corroded transverse reinforcement, *Eng. Struct.* 267 (114710) (2022) 1–14.
- [11] S. Fang, Axial compressive performance of corroded concrete columns strengthened by alkali-activated slag ferrocement jackets, *Front. Mater.* 7 (567777) (2020) 1–12.
- [12] S. Altoubat, M. Maalej, F.U.A. Shaikh, Laboratory simulation of corrosion damage in reinforced concrete, *Int. J. Concr. Struct. Mater.* 10 (3) (2016) 383–391.
- [13] ASCE, 2021 Report Card for America's Infrastructure. 2021.
- [14] Wallbank, E.J. The Performance of Concrete in Bridges: a Survey of 200 Highway Bridges. 1989.
- [15] F. Vecchi, B. Belletti, Capacity assessment of existing RC columns, *Buildings* 11 (161) (2021) 1–19.
- [16] A.S. Rajput, U.K. Sharma, K. Engineer, Seismic retrofitting of corroded RC columns using advanced composite materials, *Eng. Struct.* 181 (2019) 35–46.
- [17] A. Meda, et al., Experimental evaluation of the corrosion influence on the cyclic behaviour of RC columns, *Eng. Struct.* 76 (2014) 112–123.
- [18] M.M. Kashani, J. Maddocks, E.A. Dizaj, Residual capacity of corroded reinforced concrete bridge components: state-of-the-art review, *J. Bridg. Eng.* 24 (7) (2019) 1–16.
- [19] L. Yu, et al., Structural performance of RC beams damaged by natural corrosion under sustained loading in a chloride environment, *Eng. Struct.* 96 (2015) 30–40.
- [20] J. Rodriguez, L.M. Ortega, J. Casal, Load carrying capacity of concrete structures with corroded reinforcement, *Constr. Build. Mater.* 11 (4) (1997) 239–248.
- [21] A.S. Rao, et al., Simplified structural deterioration model for reinforced concrete bridge piers under cyclic loading, *Struct. Infrastruct. Eng.* 13 (1) (2017) 55–66.
- [22] A. Guo, et al., Experimental investigation on the cyclic performance of reinforced concrete piers with chloride-induced corrosion in marine environment, *Eng. Struct.* 105 (2015) 1–11.

- [23] F. Biondini, E. Camnasio, A. Palermo, Lifetime seismic performance of concrete bridges exposed to corrosion, *Struct. Infrastruct. Eng.* 10 (7) (2014) 880–900.
- [24] R. Aboutaha, et al., Seismic evaluation and retrofit of deteriorated, *Concr. Bridge Components* (2013).
- [25] A. Mohammed, H. Almansour, B. Martín-Pérez, Simplified finite element model for evaluation of ultimate capacity of corrosion-damaged reinforced concrete beam-columns, *Int. J. Adv. Struct. Eng.* 10 (4) (2018) 381–400.
- [26] N.S. Vu, B. Yu, B. Li, Prediction of strength and drift capacity of corroded reinforced concrete columns, *Constr. Build. Mater.* 115 (2016) 304–318.
- [27] J.B. Mander, M.J.N. Priestley, R. Park, Theoretical stress-strain model for confined concrete, *J. Struct. Eng.* 114 (8) (1988) 1804–1826.
- [28] X. Zeng, Finite element analysis of square RC columns confined by different configurations of transverse reinforcement, *Open Civil Eng. J.* 11 (2017) 292–302.
- [29] M. Saatcioglu, S.R. Razvi, Strength and ductility of confined concrete, *J. Struct. Eng.* 118 (6) (1992) 1590–1607.
- [30] X. Liang, R. Beck, S. Sritharan, Understanding the confined concrete behavior on the response of hollow bridge columns. Department of Civil Construction and Environmental Engineering, Iowa State University, 2015.
- [31] J. Hoshikuma, et al., Stress-strain model for confined reinforced concrete in bridge piers, *J. Struct. Eng.* 123 (5) (1997) 624–633.
- [32] K. Andisheh, A. Scott, A. Palermo, Effects of corrosion on stress-strain behavior of confined concrete, *J. Struct. Eng.* 147 (7) (2021) 04021087.
- [33] Y.-C.-O. Ou, D.N. Nguyen, Plastic hinge length of corroded reinforced concrete beams, *ACI Struct. J.* 111 (5) (2014).
- [34] Y.-C. Ou, H.-D. Fan, N.D. Nguyen, Long-term seismic performance of reinforced concrete bridges under steel reinforcement corrosion due to chloride attack, *Earthq. Eng. Struct. Dyn.* 42 (14) (2013) 2113–2127.
- [35] The British Standards, Steel for the reinforcement of concrete — Weldable reinforcing steel — General, in BS EN 10080:2005. 2005, BSI Standards Limited: London, UK.
- [36] The British Standards, Steel for the reinforcement of concrete — Weldable reinforcing steel — Bar, coil and decoiled product — Specification, in BS 4449-2005+A3-2016. 2016, BSI Standards Limited: London, UK.
- [37] The British Standards, Metallic materials - Tensile testing - Part 1: Method of test at room temperature, in BS EN ISO 6892-1:2019. 2020, BSI Standards Limited: London, UK.
- [38] C. Lee, et al., Accelerated corrosion and repair of reinforced concrete columns using carbon fibre reinforced polymer sheets, *Can. J. Civ. Eng.* 27 (5) (2000) 941–948.
- [39] M.K. Kumar, et al., Corrosion resistance performance of fly ash blended cement concretes, *Int. J. Res. Eng. Technol. (IJRET)* 1 (2) (2012) 448–454.
- [40] Deb, S. and B. Pradhan. A Study on corrosion performance of steel in concrete under accelerated condition. In International Conference on Structural Engineering Construction and Management. 2013. Kandy, Sri Lanka.
- [41] A.M. Al-Swaidani, S.D. Aliyan, *Effect of adding scoria as cement replacement on durability-related properties*, *Int. J. Concr. Struct. Mater.* 9 (2) (2015) 241–254.
- [42] V. Talakokula, S. Bhalla, A. Gupta, Corrosion assessment of reinforced concrete structures based on equivalent structural parameters using electro-mechanical impedance technique, *J. Intell. Mater. Syst. Struct.* 25 (4) (2014) 484–500.
- [43] M.D. Pritzl, H. Tabatabai, A. Ghorbanpoor, Laboratory evaluation of select methods of corrosion prevention in reinforced concrete bridges, *Int. J. Concr. Struct. Mater.* 8 (3) (2014) 201–212.
- [44] M.M. Kashani, A.J. Crewe, N.A. Alexander, Nonlinear stress-strain behaviour of corrosion-damaged reinforcing bars including inelastic buckling, *Eng. Struct.* 48 (2013) 417–429.
- [45] T.A. El Maaddawy, K.A. Soudki, Effectiveness of impressed current technique to simulate corrosion of steel reinforcement in concrete, *J. Mater. Civ. Eng.* 15 (1) (2003) 41–47.
- [46] T. El Maaddawy, S. Khaled, T. Topper, Analytical model to predict nonlinear flexural behavior of corroded reinforced concrete beams, *ACI Struct. J.* 102 (4) (2005) 550–559.
- [47] ASTM, G.-. Standard practice for preparing, cleaning, and evaluating corrosion test specimens, 2011, ASTM International.
- [48] Q. Li, et al., Effects of reinforcement corrosion and sustained load on mechanical behavior of reinforced concrete columns, *Materials (Basel)* 15 (10) (2022).
- [49] X.-L. Gu, et al., Corrosion of stirrups under different relative humidity conditions in concrete exposed to chloride environment, *J. Mater. Civ. Eng.* 32 (1) (2020) 04019329.
- [50] C.V. Nguyen, P. Lambert, Effect of current density on accelerated corrosion of reinforcing steel bars in concrete, *Struct. Infrastruct. Eng.* 14 (11) (2018) 1535–1546.
- [51] H.-L. Dong, et al., Axial compressive behavior of square concrete columns reinforced with innovative closed-type winding GFRP stirrups, *Compos. Struct.* 192 (2018) 115–125.
- [52] E.A. Dizaj, M.M. Kashani, Numerical investigation of the influence of cross-sectional shape and corrosion damage on failure mechanisms of RC bridge piers under earthquake loading, *Bull. Earthq. Eng.* 18 (10) (2020) 4939–4961.
- [53] M.M. Kashani, Size effect on inelastic buckling behavior of accelerated pitted corroded bars in porous media, *J. Mater. Civ. Eng.* 29 (7) (2017) 04017022.
- [54] M.M. Kashani, A.J. Crewe, N.A. Alexander, Nonlinear cyclic response of corrosion-damaged reinforcing bars with the effect of buckling, *Constr. Build. Mater.* 41 (2013) 388–400.
- [55] M.M. Kashani, et al., Phenomenological hysteretic model for corroded reinforcing bars including inelastic buckling and low-cycle fatigue degradation, *Comput. Struct.* 156 (2015) 58–71.
- [56] D. Coronelli, P. Gambarova, Structural assessment of corroded reinforced concrete beams: modeling guidelines, *J. Struct. Eng.* 130 (8) (2004) 1214–1224.
- [57] P. Li, et al., Experimental study on the mechanical properties of corroded RC columns repaired with large rupture strain FRP, *J. Build. Eng.* 54 (2022), 104413.